Optical propagation in molecular gases undergoing filamentation-assisted field-free alignment

F. Calegari, C. Vozzi, and S. Stagira*
National Laboratory for Ultrafast and Ultraintense Optical Science-CNR-INFM, Dipartimento di Fisica, Politecnico di Milano, Milano I-20133, Italy
(Received 7 October 2008; published 23 February 2009)

An intense and ultrashort laser pulse undergoing filamentation in a molecular gas induces impulsive rotational excitation of the medium. The changes produced in the gas optical properties can dramatically affect a delayed probe pulse propagating in the wake of the pump one. We observe remarkable spatial and spectral reshaping of the probe beam occurring simultaneously at suitable pump-probe delays. These effects are experimentally demonstrated in several molecular gases, with minor changes related to the nature of the medium. A theoretical investigation shows that spatial and temporal domains are strictly related and cannot be disentangled like in experiments performed in a hollow waveguide.

DOI: 10.1103/PhysRevA.79.023827 PACS number(s): 42.65.Re, 42.65.Jx, 37.10.Vz

I. INTRODUCTION

The interaction of intense and ultrashort laser pulses with molecular gases has received increasing interest in the last decade, owing to the noticeable effects induced in the medium by the impulsive Raman excitation [1]. In particular periodic revivals of molecular alignment, related to the rotational response of the gas, can be observed after interaction with the pump pulse [2]. Such effect is known as *field-free alignment* or *nonadiabatic alignment*. After rotational excitation the molecular medium loses the optical isotropy, due to random orientation of molecules, acquiring birefingence [3] and, at the same time, undergoing temporal modulation of the refractive index [4]. Owing to its peculiar features, field-free alignment (FFA) has been characterized and exploited in many ways, such as through Coulomb explosion [5], optical Kerr gating [6], cross defocusing of laser pulses [7], spectral interferometry [8,9], and time resolved polarigraphy [10].

Nowadays, FFA is a basic tool for experimental investigations in molecular physics, like for instance in ionization of aligned molecules [11], controlling of high-order harmonic generation [12–14], and in molecular orbital tomography [15]. Numerous applications to nonlinear optics have been proposed such as dynamic quasi phase matching of nonlinear optical processes [3,16], pulse spectral broadening in gas-filled hollow waveguides [4,17], self-compression in high pressure gas cells [18], phase shaping of ultrashort pulses [19,20], and realization of active laser media in the terahertz region [21]. FFA plays also a crucial role in the long-range propagation of laser pulses in the atmosphere [22,23].

In spite of the large interest and the numerous applications of FFA in physics and nonlinear optics, still few experiments have considered in detail the spatiotemporal effects occurring in the free propagation of laser pulses through impulsively aligned molecular gases [24]. Recently, the authors showed that a light probe pulse propagating in nitrogen along the wake of an optical filament undergoes a strong spatial collapse and a huge spectral broadening at suitable time delays with respect to the filamenting pulse [25]. This finding was ascribed to FFA of nitrogen molecules, inducing spatiotemporal effects on the probe along the filament wake.

In this work we extend the above-mentioned study, showing that the experimental findings of Calegari *et al.* [25] are not limited to nitrogen, but are reproducible in several gases of linear molecules, with minor changes related to the nature of the medium under investigation. The observed effects were studied both experimentally and theoretically, allowing a clear interpretation of the mechanism of pulse propagation in a gas undergoing filament-assisted field-free alignment (FA-FFA). Our simulations predict that FA-FFA induces a strong spatiotemporal reshaping of a probe pulse propagating in the excited medium; this finding has to be compared with experiments performed in hollow waveguides [4], where probe spectral broadening is the main observed effect.

The paper is organized as follows: after description of setup and experimental findings in Sec. II, we present in Sec. III a theoretical model for the interpretation of experimental observations; afterwards, on the basis of numerical simulations, we discuss about optical propagation in a molecular gas undergoing FA-FFA. We then summarize the results in Sec. IV.

II. SETUP AND EXPERIMENTAL RESULTS

The experiments have been performed using a Ti:sapphire laser system in chirped pulse amplification, generating 800–nm, 60–fs pulses at 10 Hz. A small fraction (about 1 mJ) of the laser beam was split in two arms as shown in Fig. 1: the first one (with a maximum energy of 0.9 mJ) was focused in a gas cell by a 60-cm focal length lens, generating a short-range optical filament. An iris was used to tune the pump power for stable filamentation in the gas; typical pump powers ranged between 300 and 450 μJ according to gas composition and pressure. The length of the visible plasma trace generated by the filamentation process was on the order of 4 cm in our experimental conditions.

The second pulse was frequency doubled in a 1-mm-thick β-barium borate (BBO) crystal followed by an IR-absorbing filter (maximum second harmonic energy: 10 μJ) and fo-

*salvatore.stagira@fisi.polimi.it

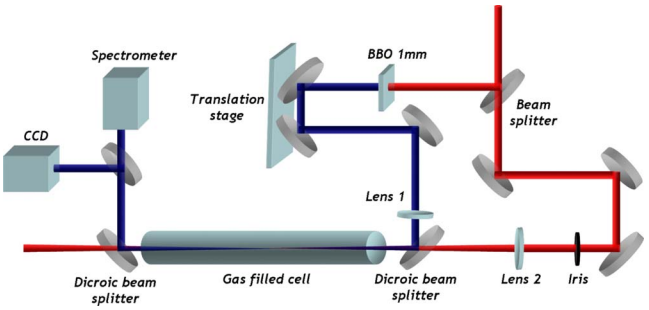

FIG. 1. (Color online) Experimental setup.

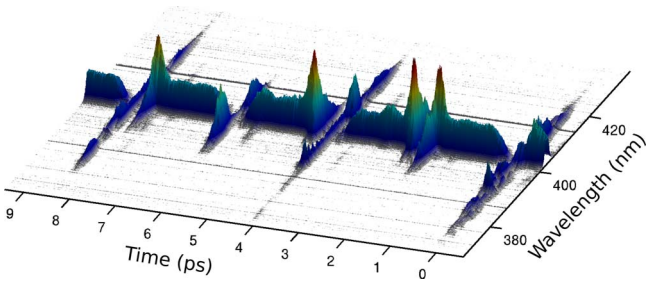

FIG. 2. (Color online) Temporal evolution of the output probe spectrum in N_2. Pump and probe polarizations were parallel.

cused by a 30-cm focal length lens in order to probe the effects occurring in the filament wake. Owing to the limited phase matching bandwidth, the transform limited probe duration, as evaluated from the spectrum, resulted in about 80 fs. A half-wave plate was used to change the polarization direction of the pump with respect to the probe. After independent focusing, the pump and the probe pulses were collinearly combined with a dichroic beam splitter in order to overlap the two foci inside the gas cell. The gas pressure was chosen between 1 and 3 bar in order to optimize the interaction between the two beams; a computer-driven translation stage on the probe arm was used to scan the pump-probe delay. The probe beam at the output of the cell was then separated from the pump using a second dichroic beam splitter. The spatial shape and the spectrum of the probe were recorded as a function of pump-probe delay; probe images were acquired using a low noise CCD camera; spectra were acquired selecting the central part of the beam with an optical fiber coupled to a spectrometer. The experiments discussed in this work were performed in N_2, O_2, and CO_2; although not reported here, we observed spatiotemporal effects also in FA-FFA performed in N_2O and H_2.

A. Temporal phase modulation and probe spectral broadening

In a set of experiments we analyzed the spectral modulation induced by the filament-assisted FFA on the probe beam. It is useful to introduce the ideal temporal compression factor $\beta=\tau_0/\tau$, defined as the ratio between the transform-limited probe temporal duration without (τ_0) and with (τ) pump excitation, respectively; β was calculated from the acquired spectra. This factor gives at the same time an idea of the probe spectral broadening and of the temporal compression that could be achieved after ideal compensation of probe dispersion at the output of the gas cell.

Figure 2 shows the probe pulse spectrum measured in nitrogen at a pressure of 3 bar as a function of the pump-probe delay; in this case the pump and probe polarization directions were parallel. The probe undergoes remarkable spectral broadening at periodic delays, corresponding to integer and fractional multiples of the rotational period $T_{N_2} \approx 8.4$ ps, owing to the temporal refractive index modulation occurring in the filament wake. In order to quantify the observed broadening we calculated the β factor along the measured spectral scan; β is larger in correspondence of full and half revivals of alignment ($\beta \approx 11-12$), whereas it is smaller in correspondence of quarter revivals ($\beta \approx 4-6$). A strong effect ($\beta \approx 13$) is also observed when pump and probe pulses are overlapped in time, owing to the instantaneous cross-phase modulation induced on the probe by Kerr effect; this instantaneous effect is followed by a delayed response, producing a noticeable spectral broadening up to few hundreds of femtoseconds later.

It is worth noting that spectral broadening induced by rotational excitation has been already observed in pump-probe measurements performed in a hollow waveguide [4]; nevertheless in those experiments the length of the waveguide ranged between 30 and 60 cm, which is 1 order of magnitude longer than the vacuum Rayleigh range of the filamenting pump beam used in our setup. The amount of spectral broadening we observed is not compatible with a free propagation of the probe, since its natural divergence would strongly limit the interaction with the filament wake. As it will be discussed in the following, we ascribe the observed behavior to the occurrence of spatiotemporal effects in the filament wake [25].

The experiment was repeated at the same pressure for a pump polarization perpendicular to the probe one; the corresponding probe spectrum is shown in Fig. 3. In this case the measured effect was much weaker with respect to the case of parallel polarizations: periodic revivals of spectral broadening are still observed, but the ideal compression factor is $\beta \approx 5$ around the full revival. As discussed in Sec. III, the refractive index modulation in the case of pump and probe having perpendicular polarizations is half the amount obtained in the configuration with parallel polarizations; this is consistent with the observed value of β.

The experiments performed in N_2 were also reproduced in other molecular gases, namely, O_2 and CO_2. Figure 4 shows

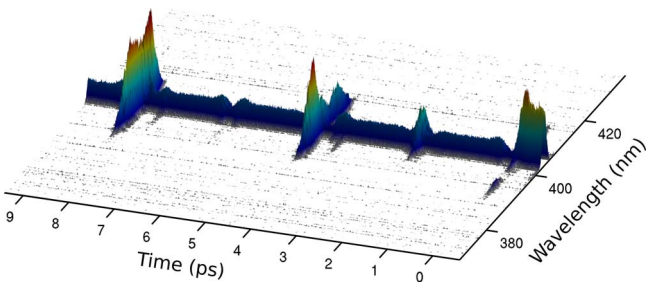

FIG. 3. (Color online) Temporal evolution of the output probe spectrum in N_2. Pump and probe polarizations were perpendicular.

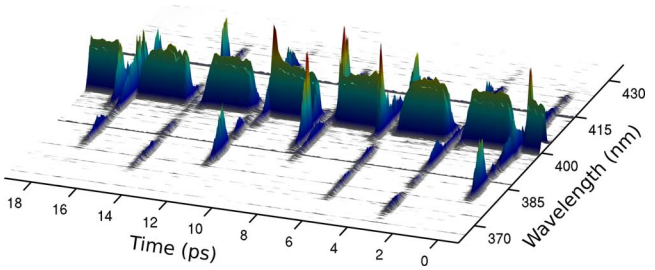

FIG. 4. (Color online) Temporal evolution of the output probe spectrum in O_2. Pump and probe polarizations were parallel.

the evolution of the probe spectrum in O_2 at a pressure of 2 bar as a function of pump-probe delay, for the case of parallel polarizations. Also in this case the probe undergoes remarkable spectral broadening at periodic delays, corresponding to integer and fractional multiples of the rotational period $T_{O_2} \approx 11.6$ ps. Differently from the nitrogen case, the amount of spectral broadening observed in correspondence of full and half revivals is comparable to that observed on quarter revivals, as one can note from the figure. A compression factor $\beta \approx 14-15$ was for instance measured around both the first quarter and the half revival. This peculiarity is related to the statistics of rotational population: differently from N_2, where thermal population of even and odd rotational levels is distributed with a 2:1 ratio, in O_2 only odd rotational states are occupied. Correspondingly, the quarter revivals in oxygen have the same intensity than half and full revivals, whereas in nitrogen a partial cancellation occurs owing to opposite contribution to quarter revivals from even and odd states.

We observed spectral broadening also in carbon dioxide; the probe spectrum, measured at a pressure of 1 bar in the case of pump and probe with parallel polarizations, is shown in Fig. 5. Revivals corresponding to integer and fractional multiples of the rotational period $T_{CO_2} \approx 42.7$ ps were observed. Although the behavior is similar to that of N_2 and O_2, a smaller amount of spectral broadening ($\beta \approx 6$ around the first quarter revival) was measured in this case. This lower effect cannot be completely ascribed to the lower pressure used for CO_2 with respect to others gases. Indeed it must be observed that the polarization anisotropy of carbon dioxide is 2.79 times the one of N_2 and 1.82 times the one of O_2 [26]. Thus the product density × anisotropy (which is the relevant parameter for spectral broadening [4]) was similar in the three experiments; moreover numerical simulations per-

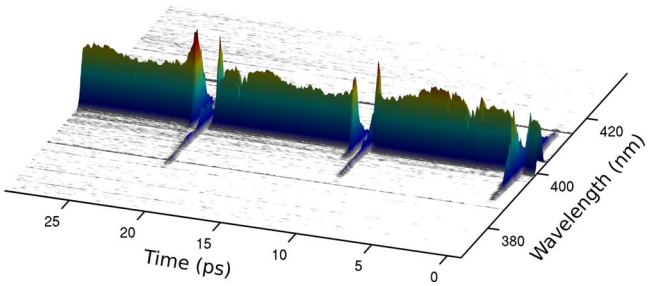

FIG. 5. (Color online) Temporal evolution of the output probe spectrum in CO_2. Pump and probe polarizations were parallel.

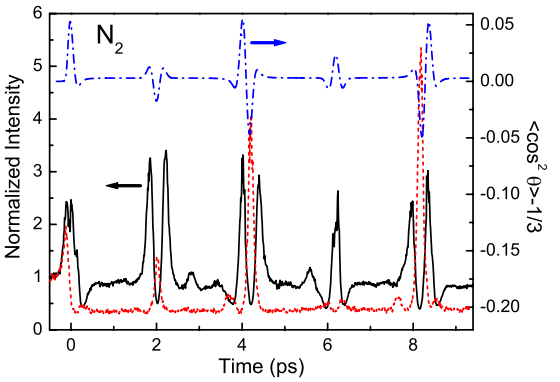

FIG. 6. (Color online) Temporal evolution of the spectrally integrated probe signal in N_2 (left scale); solid line: pump and probe polarizations are parallel; dashed line: polarizations are perpendicular. Dash-dotted line: alignment factor calculated in the experimental conditions (right scale).

formed in the experimental conditions show that the amount of FFA was comparable in the three cases. Accordingly, one should expect comparable spectral broadenings in the three gases, whereas similar results are observed only in nitrogen and oxygen. The reduced broadening observed in CO_2 can be ascribed to its smaller rotational constant with respect to the other two gases. Indeed, owing to a larger inertia, rotational revivals in CO_2 are much slower; thus the spectral broadening induced on the probe (which is as a first approximation related to the second temporal derivative of the probe phase) is weaker with respect to lighter gases. Differences among the filamentation dynamics in the three gases should be also considered for a complete explanation of the results.

B. Spatial modulation of the probe beam

A careful analysis of Figs. 2–5 shows that the spectrally integrated probe signal is not conserved as a function of pump-probe delay; this result appears incorrect at first sight, because we are dealing with a pure phase modulation, which should not perturb the probe energy. Since the spectrum was measured in the center of the probe beam, this finding can be explained as the result of a spatial modulation of the probe, which changes the coupling of the beam with the spectrometer input. As an example, we report in Fig. 6 the spectrally integrated probe signal acquired in nitrogen as a function of pump-probe delay for pump and probe polarizations in the parallel configuration (solid line) and the perpendicular one (dashed line). The two curves are normalized to the probe signal at negative pump-probe delays (scale on the left). The signal measured for perpendicular polarizations shows a complementary evolution with respect to the case of parallel polarizations. We show in the same figure the molecular alignment factor $\langle \cos^2 \theta \rangle$ (dash-dotted line, scale on the right) calculated in the experimental conditions; the curve is vertically displaced for clarity. A direct comparison between the probe signal and the alignment factor is instructive: for parallel polarizations the maxima of probe signal correspond to maxima of alignment; the opposite occurs for the configuration with perpendicular polarizations.

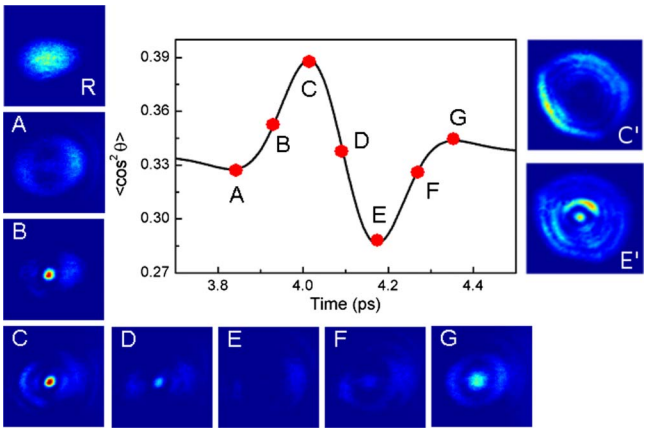

FIG. 7. (Color online) Probe spatial characterization in N_2. Main panel: temporal evolution of the alignment factor calculated in the core of the filament. Smaller panels: (R) unperturbed probe profile; (A-G) probe spatial profile for parellel polarizations, (C′,E′) probe profile for perpendicular polarizations.

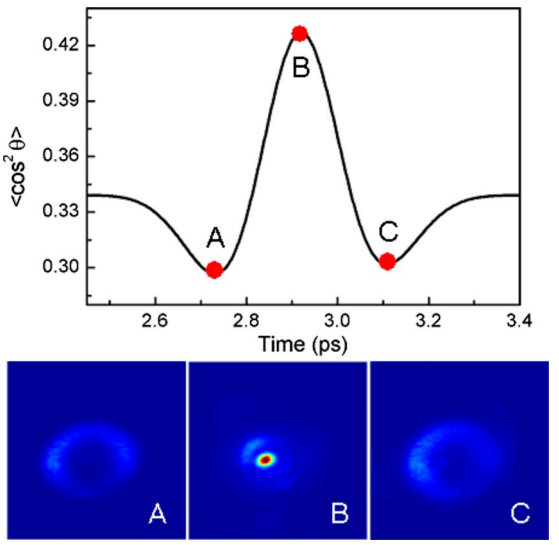

FIG. 8. (Color online) Probe spatial characterization in O_2. Main panel: temporal evolution of the alignment factor calculated in the core of the filament. Smaller panels: probe spatial profile; pump and probe polarizations were parallel.

Such behavior can be understood as follows: for a probe pulse polarized along the molecular alignment axis (that is, along the polarization direction of the pump), a spatial collapse of the probe at maximum alignment and a defocusing at minimum alignment occur. For a probe pulse polarized perpendicularly to the molecular alignment axis, we observe the opposite evolution. These spatial modulations are responsible for changes in the probe coupling to the spectrometer input. A further indication of spatial effects is clearly seen both in Figs. 3 and 6 for the case of perpendicular polarizations: for positive delays the probe signal reduces significantly with respect to the initial value even far from revival occurrences; this effect is much weaker for parallel polarizations. We attribute such behavior to the increased incoherent molecular alignment inside the filament wake, which is present also away from the rotational revivals: for perpendicular polarizations the incoherent alignment induces a defocusing of the probe beam which is added to the weak defocusing due to the plasma left by pump filamentation; the result is a reduction in the probe signal detected by the spectrometer. On the contrary, for parallel polarizations the plasma defocusing and the effect of the incoherent alignment cancel each other. It must be pointed out that, in the experimental conditions we adopted, the effects of plasma defocusing were always much weaker than those induced by molecular alignment during rotational revivals.

In order to quantify in a more rigorous way these spatial effects, we recorded the spatial profile of the probe as a function of pump-probe delay. A set of measurements was performed in nitrogen, keeping the pump and probe polarizations parallel. The panel marked as R in Fig. 7 shows the unperturbed probe beam at the output of the cell, whereas panels from A to G display the same pattern for some pump-probe delays around the first half revival (~4.2 ps). The calculated evolution of the molecular alignment $\langle \cos^2 \theta \rangle$ in the central region of the filament wake is shown in the main panel of Fig. 7. For a delay coincident with the maximum of the half revival (C), the probe beam collapses at the center of the filament wake, as shown in the corresponding small panel; we estimated that about 30% of the input energy is transferred to the collapsed beam. For a pump-probe delay corresponding to the minimum of the half revival (E), the probe beam assumes an annular shape as displayed in the corresponding panel. Smaller effects are also present at time delays corresponding to the local minimum and the local maximum of the half revival.

We performed also measurements for pump polarization perpendicular to the probe one; the spatial effects, though visible, were weaker as expected from the lower refractive index modulation experienced by the probe in this configuration [see Eq. (3) in Sec. III]. The experiment revealed an opposite behavior with respect to the parallel configuration: the probe develops a ring feature in correspondence of maximum alignment (as shown in the panel marked as C′) whereas a central spot appears in correspondence of minimum alignment (panel E′).

The spatial characterization of the probe beam was considered also in O_2 and CO_2. Figure 8 shows some probe profiles acquired around the first quarter revival in O_2, at about 2.9 ps time delay; the evolution of the alignment factor is also shown. Pump and probe polarizations were parallel. Again, the probe collapses in the center of the filament wake for a delay corresponding to maximum alignment (point B in the figure), whereas it acquires an annular shape in correspondence of minimum alignment (points A and C).

Similar results were obtained in carbon dioxide, as shown in Fig. 9. Also in this case the probe profiles were acquired around the first quarter revival, at a pump-probe delay of about 10.7 ps. Pump and probe polarizations were kept parallel. Note that in the ground vibrational state of CO_2 only even rotational levels are occupied; indeed, comparing Fig. 8 with Fig. 9, we can see that there is a complementary behavior in CO_2 with respect to O_2, since in carbon dioxide we observe two local maxima of alignment instead of only one. Besides this difference, the probe appears again collapsed in

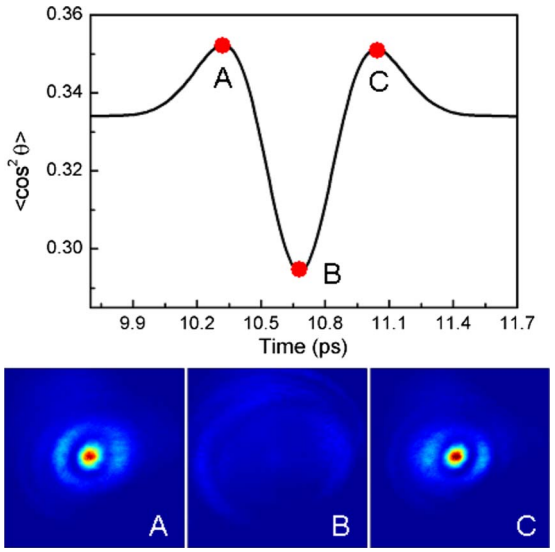

FIG. 9. (Color online) Probe spatial characterization in CO_2. Main panel: temporal evolution of the alignment factor calculated in the core of the filament. Smaller panels: probe spatial profile; pump and probe polarizations were parallel.

the center of the filament wake at maximum alignment (points A and C in the figure), whereas it acquires an annular shape in correspondence of minimum alignment (B).

We can summarize the experimental results of this section as follows: the probe undergoes spatial confinement when the refractive index increases above the unperturbed value $\bar{n}$, which corresponds to random molecular alignment. This effect occurs at alignment maxima for probe polarization parallel to the alignment axis, whereas it is seen at alignment minima for perpendicular polarization. Such behavior is consistent with the refractive index evolution expected in the excited medium [see Eq. (3) in Sec. III]. Beam defocusing is instead observed when refractive index decreases below $\bar{n}$.

The nature of this effect will be discussed more deeply in the following section; here we limit ourselves to state that the refractive index profile induced in the medium changes along the transverse direction according to the pump spatial profile. Since the pump intensity is higher in the center of the beam, the change in refractive index will be maximized on the filament axis. Thus a guiding profile will develop when refractive index increases with respect to $\bar{n}$; an antiguiding profile will be obtained when it decreases below $\bar{n}$. These transient refractive index profiles are responsible for the observed spatial modulations of the probe beam [25].

III. THEORETICAL MODEL

Optical filamentation is a propagation effect in which a laser pulse is self-guided, creating a channel where the pulse intensity is clamped [27] and the ionization is kept at a very low level. In a molecular medium, an impulsive excitation of rotational wave packet also takes place along the channel [2]. As previously mentioned, the transverse refractive index profile induced by FA-FFA could affect substantially the probe propagation, thus accounting for the remarkable spectral broadening reported in Sec. II A. The strong spatial probe modulation observed experimentally is a further evidence for this hypothesis. Nevertheless the experimental observations cannot provide a direct description of the probe evolution along the pump wake. In order to interpret the experimental results and to describe the spatiotemporal probe modification occurring inside the filament channel, we developed a numerical model in cylindrical symmetry for the propagation of pump and probe pulses in the molecular medium. We choose nitrogen as a model, since details about dispersion [28] and Kerr nonlinearity [29] in this gas can be found in the literature. The pump and probe simulated properties were chosen in order to mimic the experimental configuration. We stress that the conclusions drawn here are not limited to N_2, but can be applied with minor changes to every gas of linear molecules.

A. Propagation equations

The pump filamentation process was modeled solving the nonlinear propagation equation for the envelope of the pump electric field $\mathbf{E}_p=\mathrm{Re}\{\mathcal{E}_p(r,Y,t)\exp[i(\omega_p t-k_p Y)]\}\mathbf{u}_Z$ in the slowly varying envelope approximation (SVEA),

$$\partial_Y \mathcal{E}_p + \frac{i}{2k_p}\nabla_\perp^2 \mathcal{E}_p + i\hat{D}\mathcal{E}_p + i\frac{k_p n_2}{2\mu_0 c}|\mathcal{E}_p|^2\mathcal{E}_p - \frac{i}{2k_p}\left(\frac{\omega_{\mathrm{pl}}^2(r,t)}{c^2}\mathcal{E}_p\right) = 0, \quad (1)$$

where $\mathbf{u}_Z$ is the unity vector of the Z axis in the laboratory frame, k_p and ω_p are the pump wave number and frequency, respectively, Y is the propagation coordinate, t is the local time, n_2 is the nonlinear Kerr index, $\hat{D}$ is the dispersive operator, and $\omega_{\mathrm{pl}}(r,t)=\sqrt{\rho(r,t)e^2/m_e\varepsilon_0}$ is the instantaneous plasma frequency which takes into account multiphoton ionization effects. The evolution of the electron density $\rho(r,t)$ was determined by solving the relation

$$\partial_t \rho = (\rho_{at}-\rho)\sigma_K|\mathcal{E}_p(r,t)|^{2K}, \quad (2)$$

where σ_K is the cross section for multiphoton ionization, K is the number of absorbed photons required for multiphoton ionization, and ρ_{at} the initial gas density; note that the pulse intensity is related to the electric field envelope by $I=c\varepsilon_0|\mathcal{E}_p|^2/2$.

The Raman contribution to the pump propagation was neglected. It is worth noting that Eq. (1) does not consider effects like spatiotemporal coupling in the Laplacian operator and in the Kerr term [25], as well as higher order nonlinearities and energy absorption by plasma generation [30]. Moreover, owing to our experimental conditions, avalanche ionization and plasma recombination were neglected in Eq. (2). In spite of these approximations, such equations represent a reasonable compromise between computational time and description of short-range filamentation. We integrated Eqs. (1) and (2) in the case of nitrogen with the following parameters: pump wavelength $\lambda_p=800$ nm; Gaussian temporal distribution, with pulse energy $\mathfrak{E}_p=250$ μJ and duration $\tau_p=60$ fs; Gaussian spatial profile with a focal spot radius $w_{0p}=90$ μm in vacuum [31]. The resulting pump pulse distribution was used to determine the evolution of the molecu-

lar alignment factor $\langle\cos^2\theta\rangle(r,t,Y)$ with respect to the alignment axis Z, according to procedures reported in [2,32].

The refractive index modulation was then calculated according to the following relations, which are valid in a gaseous medium [8]:

$$n_X(\mathbf{r},t) = \bar{n} + \frac{N\Delta\alpha}{4\varepsilon_0}\left[\frac{1}{3} - \langle\cos^2\theta\rangle(\mathbf{r},t)\right],$$

$$n_Z(\mathbf{r},t) = \bar{n} + \frac{N\Delta\alpha}{2\varepsilon_0}\left[\langle\cos^2\theta\rangle(\mathbf{r},t) - \frac{1}{3}\right], \quad (3)$$

where $\bar{n}$ is the refractive index for random molecular orientation, corresponding to $\langle\cos^2\theta\rangle = 1/3$, and N is the molecular density. $\Delta\alpha = \alpha_\parallel - \alpha_\perp$, where $\alpha_\parallel$ and $\alpha_\perp$ are the components of the polarizability tensor parallel and perpendicular to the molecular axis, respectively. It must be noted that, after impulsive excitation, the refractive index modulation along the two axes always obeys to the relation $\Delta n_X = -\Delta n_Z/2$ [33].

The resulting refractive index evolution was then used to model the propagation of the probe beam inside the filament wake. Self-focusing and dispersion contributions to the probe propagation were not considered, since the essence of the investigated effect is dominated by the FFA; the effects of plasma generated by the filamenting pulse were included in the probe equation. The evolution of the envelope of the probe pulse $\mathbf{E}_{\rm pr} = \mathrm{Re}\{\mathcal{E}_{{\rm pr},m}(r,Y,t)\exp[i(\omega_{\rm pr}t - k_{\rm pr}Y)]\}\mathbf{u}_m$ was modeled as

$$\partial_Y\mathcal{E}_{{\rm pr},m} + \frac{i}{2k_{\rm pr}}\nabla_\perp^2\mathcal{E}_{{\rm pr},m} + ik_{\rm pr}[n_m(r,Y,t) - \bar{n}]\mathcal{E}_{{\rm pr},m} - \frac{i}{2k_{\rm pr}}\left(\frac{\omega_{\rm pl}^2(r)}{c^2}\mathcal{E}_{\rm pr}\right) = 0, \quad (4)$$

where $\mathbf{u}_m$ is the unity vector of the laboratory axis m, $m = \{X,Z\}$, $k_{\rm pr}$ and $\omega_{\rm pr}$ are the probe wave number and frequency, respectively. It is worth noting that the plasma frequency in Eq. (4) was calculated according to the electron density left by the pump pulse and depends only on the radial position, since we neglected plasma recombination as well as ionization induced by the probe pulse. The probe equation was solved assuming a wavelength $\lambda_{\rm pr} = 400$ nm and a Gaussian distribution both in temporal and spatial domains, with, respectively, a duration $\tau_{\rm pr} = 80$ fs and a focal spot radius $w_{0\rm pr} = 55$ μm in vacuum; since nonlinear self-effects were neglected, the probe energy is not relevant for these simulations. Both Eqs. (1) and (4) were integrated exploiting a Fourier-Hankel split-step algorithm in a simulation box of 40 cm $\times$ 1.5 mm; the pump focus was set in the middle of the box. Pump and probe evolution were determined assuming a nitrogen pressure of 3 bar at room temperature.

B. Pump filament evolution

We show in Fig. 10(b) the simulated evolution of the on-axis filamenting pump fluence $\mathcal{F}_p(0,Y) = \int_{-\infty}^{\infty} c\varepsilon_0|\mathcal{E}_p(0,Y,t)|^2/2dt$ (solid line) and of the on-axis ionization level (dash-dotted line). As can be seen, the ionization is always much lower than 1%, thus allowing to neglect the population depletion in our model. The fluence $\mathcal{F}$ is a good representation of the filament evolution and, for the pump duration considered here, it gives also a measure of the induced molecular alignment, since the latter depends mainly on $\mathcal{F}_p(r,Y)$ and weakly on the actual pump duration [34]. As can be seen from the figure, a channel of clamped fluence with a small overshoot is formed along the propagation axis, with a full width at half maximum of about 6 cm in longitudinal direction; the result can be compared with the fluence evolution under vacuum (dashed line). The simulation proves that filamentation sustains a larger fluence (thus a larger molecular alignment) for an extended range with respect to the standard Gaussian propagation. The minimum channel radius at half maximum is on the order of 30 μm (see Fig. 10, panel A), thus well fitting the dimensions of the simulated probe beam in the focal region.

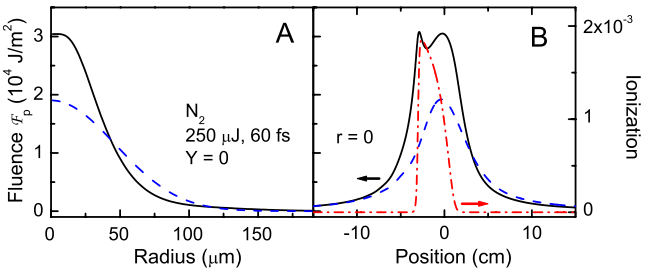

FIG. 10. (Color online) Simulated (a) radial and (b) longitudinal fluence evolution in N_2 of the filamenting pump (solid line, left scale). The dashed line shows the pump fluence in vacuum. Dash-dotted line: ionization level along the propagation axis (right scale).

C. Probe propagation at maximum alignment

A simulation was performed fixing the pump-probe delay at 4.12 ps (around the maximum alignment on the half revival of nitrogen), setting the pump and probe polarizations parallel and calculating the probe evolution inside the pump filament wake. In order to optimize the probe-wake coupling, the probe focus was placed 2.5 cm upstream the pump one. Figure 11 shows the simulated probe fluence $\mathcal{F}_{\rm pr}(r,Y) = \int_{-\infty}^{\infty} c\varepsilon_0|\mathcal{E}_{\rm pr}(r,Y,t)|^2/2dt$ calculated (a) without and (b) with the occurrence of FA-FFA induced by the pump. Note that the color scale is different in the two panels. As clearly seen, the refractive index modulation induced by FA-FFA creates a guiding channel, in which the probe propagates for about 6 cm. Interestingly, this is also the filament channel length (see Fig. 10). One can see that the probe undergoes some refocusing cycles probably due to the short channel length, not sufficient for stabilizing the guided propagation. A contribution to such refocusing from the pump fluence overshoot (see Fig. 10) could be also present. It is worth noting that the weak plasma defocusing, which is taken into account, does not hinder the guiding effect induced on the probe by molecular alignment. The far-field probe profile (not shown) reveals that a beam collapse is observed at large distance with respect to the unperturbed configuration, thus confirming the experimental result.

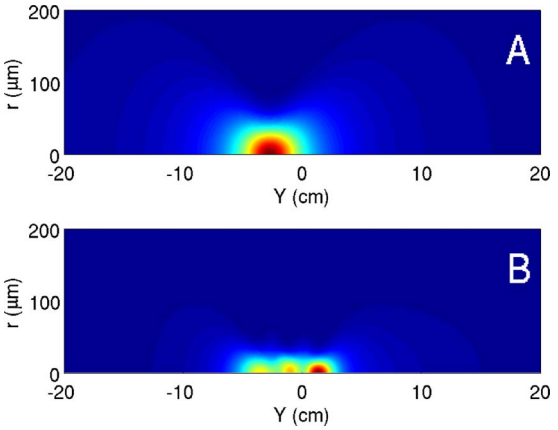

FIG. 11. (Color online) Simulated probe fluence in N_2 (a) without and (b) with filamentation-assisted FFA, as a function of propagation distance and radius. The pump-probe delay is set at 4.12 ps; the color scale is different in the two panels.

Figure 12 shows in detail the simulated temporal behavior of the probe pulse along the propagation axis (thus in $r=0$). The transient refractive index change Δn calculated in the center of the box $(Y=0, r=0)$ is reported for comparison as a function of the local time in panel A. Since the probe pulse lasts 80 fs, it fits inside the positive hemicycle of $\Delta n(t)$. Panel B shows the evolution of the probe temporal phase as a function of Y; one can see that the nonlinear phase modulation induced by the transient change Δn increases rapidly in the channel region. This result is expected, since the temporal refractive index modulation is larger inside the filament channel. Moreover the phase contour map shows a clear signature of pulse spectral broadening, since the phase has opposite slopes on the two pulse sides.

Panel C in Fig. 12 shows nevertheless a completely unexpected behavior in the normalized pulse intensity profile: the pulse duration is almost constant before entering the filament channel, but afterwards it starts oscillating. A direct comparison with Fig. 11 reveals that the probe pulse is shorter in

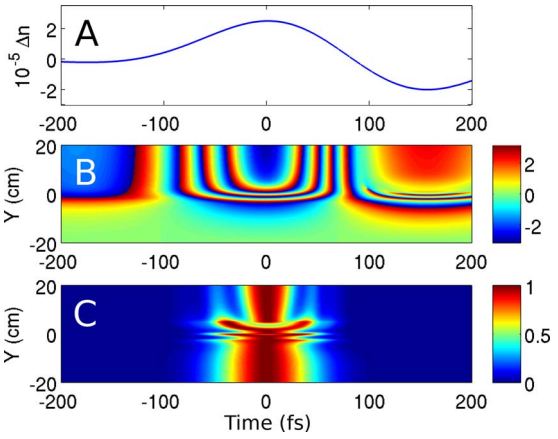

FIG. 12. (Color online) Simulated temporal behavior of the probe pulse in the wake of the pump filament; pump-probe delay is set at 4.12 ps. (a) Refractive index change in the middle of the simulation box $(r=0, Y=0)$; (b) on-axis probe field phase; (c) on-axis normalized probe field intensity.

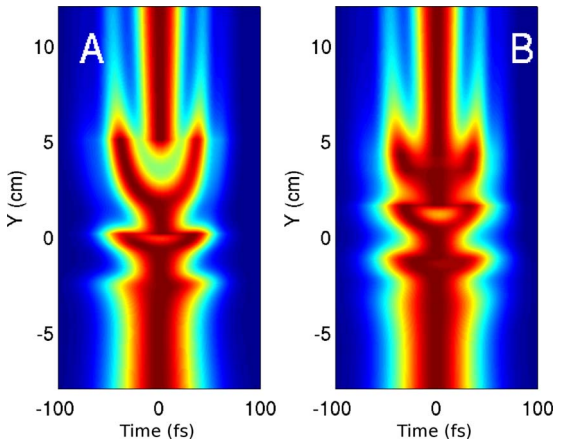

FIG. 13. (Color online) Detail of the simulated temporal probe pulse evolution in the wake of the pump filament; pump-probe delay is set at 4.12 ps. (a) Normalized probe field intensity at $r=0$ μm; (b) normalized probe field intensity at $r=30$ μm. The color scale is different in the two panels.

correspondence of beam refocusing; in particular, we found that the probe duration decreases from 80 down to 57 fs in the last refocusing stage. After that point the temporal profile reshapes in a complicated way. It must be noted that, in the limit of the SVEA approach and neglecting dispersion, this temporal reshaping could not be observed for a probe beam propagating in a gas-filled hollow waveguide; indeed in the latter case there would be only a temporal phase modulation of the probe, without any change in the pulse intensity envelope. The mechanism responsible for the observed temporal shortening is the interplay between spatial and temporal probe modulation: at the peak of the probe pulse $(t=0)$, corresponding to maximum molecular alignment, the beam is conveyed toward the wake axis owing to the convex transverse profile of refractive index; on the other hand the pulse temporal wings, exposed to a lower level of alignment, are not involved in this process. The result is a relevant increase in on-axis probe intensity around maximum alignment, which appears as temporal compression.

In order to prove this interpretation, we show in Fig. 13 a detailed view of the normalized probe temporal profile calculated on the wake axis ($r=0$ μm, panel A) and far from the axis ($r=30$ μm, panel B). One can see that in correspondence of each refocusing cycle, a pulse shortening appears on the axis, whereas a complementary temporal broadening appears far from the axis. This effect is due to the partial transfer of energy from the periphery to the center of the beam during maximum alignment (around $t=0$); the process results in a partial depletion of the pulse intensity at the beam periphery (appearing as temporal broadening of the probe) in correspondence of temporal compression at the probe center.

We also analyzed the spectral evolution of the probe along the filament wake; Fig. 14 shows the normalized probe spectrum calculated in $r=0$ as a function of the propagation distance. As can be seen from the figure, a huge spectral broadening develops suddenly in a very short range $(-4 \leq Y \leq 2$ cm) corresponding to the filament channel; at the output of the channel only minor changes in the spectral features are observed. It is worth noting that the ideal compression factor

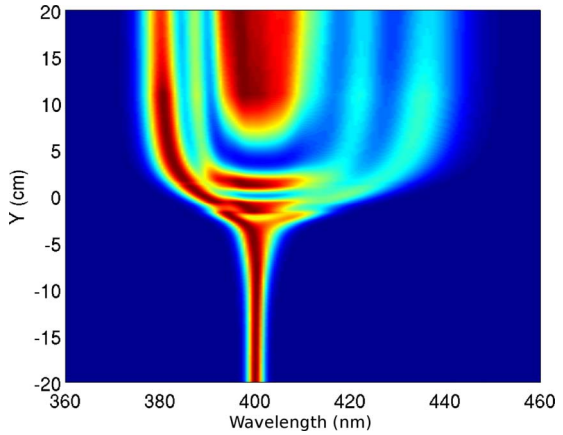

FIG. 14. (Color online) Simulated evolution of the normalized probe spectrum in the wake of the pump filament at $r=0$; pump-probe delay is set at 4.12 ps.

β at the output of the simulation box is 11.5, which is of the same order of magnitude of that measured in nitrogen. If ideally compressed, the probe duration would be about 6.9 fs.

D. Probe propagation at minimum alignment

A second simulation was devoted to the analysis of probe propagation in correspondence of the molecular alignment minimum (which is also known as *antialignment condition*). Figure 15 shows the probe fluence $\mathcal{F}_{pr}(r,Y)$ calculated (a) with and (b) without the occurrence of FFA induced by the pump; the pump-probe delay was set at 4.27 ps (around the minimum alignment on the half revival of nitrogen), pump and probe polarizations were parallel. Note that the color scale is different in the two panels. One can clearly see that, under pump excitation, the probe beam is almost completely deviated from the center just before entering the region of the filament channel. This beam deflection is due to the lower refractive index induced on the wake axis by the molecular antialignment with respect to the surrounding gas. The far-field probe profile (not shown) reveals that, at large distance, the beam assumes an annular shape with respect to the unperturbed configuration, in agreement with the experimental observation.

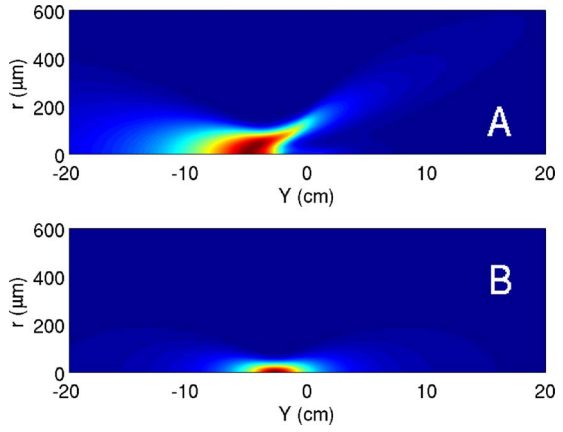

FIG. 15. (Color online) Simulated probe fluence in N_2 (a) with and (b) without filamentation-assisted FFA, as a function of propagation distance and radius. The pump-probe delay is set at 4.27 ps; the color scale is different in the two panels.

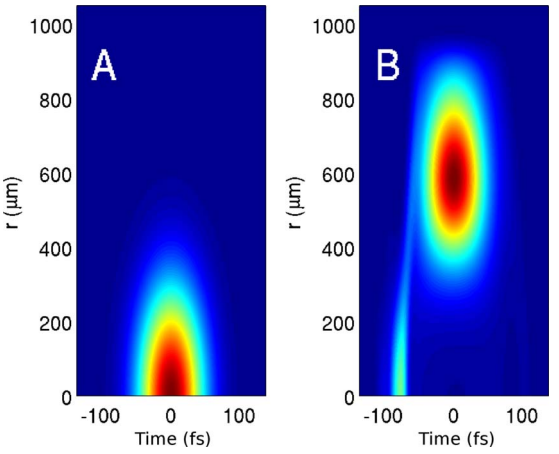

FIG. 16. (Color online) Probe intensity profile in nitrogen at the (a) input and at the (b) output of the simulation box, as a function of time and radial position. The pump-probe delay is set at 4.27 ps; the color scale is different in the two panels.

As a matter of fact, a careful inspection of the fluence evolution shows that a small fraction of the beam survives along the propagation axis; at first sight this could be considered as a small "optical leakage" through the defocusing transient structure produced by FA-FFA. Nevertheless this weak on-axis component is the proof that temporal and spatial aspects of the probe propagation cannot be separated. Indeed such mutual dependence appears clearly from the spatiotemporal analysis of the simulated probe intensity profile, as shown in Fig. 16. One can see that at the input of the simulation box (panel A) the probe pulse is confined to the propagation axis. At the end of the simulation (panel B) almost the entire pulse has been deviated 600 μm away from the axis, but a small portion on the leading edge of the pulse has propagated along the wake axis. The origin of such spatiotemporal slicing of the probe pulse has to be ascribed to the temporal evolution of the refractive index in the filament wake.

To get an insight into the probe evolution under molecular antialignment, we show in Fig. 17 the calculated dynamics of pulse propagation along the wake axis; the transient refractive index change Δn in the center of the box $(Y=0, r=0)$ is reported for comparison as a function of the local time in panel A. Panel B of Fig. 17 shows the evolution of the probe temporal phase as a function of Y; the isophase line parallel to the Y axis at $t=-70$ fs marks the transition from a positive to a negative Δn. An additional transition can be found at $t=107$ fs, though less clear. These two frontiers can be thought of as regions of quasiunperturbed refractive index.

Keeping this fact in mind, we show in panel C of Fig. 17 the temporal evolution of the on-axis normalized probe field intensity. The pulse propagates unperturbed up to the input of the filament channel; at about $Y=-4$ cm the main part of the pulse is deviated off-axis and disappears from the map. Nevertheless a small temporal slice of the pulse, centered at

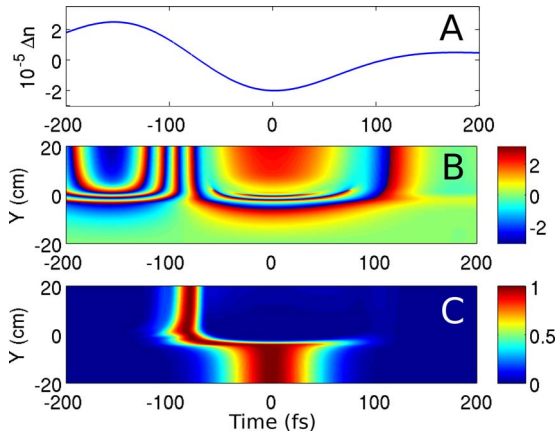

FIG. 17. (Color online) Simulated temporal behavior of the probe pulse in the wake of the pump filament; pump-probe delay is set at 4.27 ps. (a) Refractive index change in the middle of the simulation box ($r=0$, $Y=0$); (b) on-axis probe field phase; (c) on-axis normalized probe field intensity.

$t=-80$ fs with a duration of about 30 fs, survives and propagates on-axis. It is worth noting that such pulse slicing corresponds to the region of small refractive index change, as already mentioned. We can thus conclude that the weak on-axis pulse slice survives to the transient beam deflection because it corresponds to a "calm region" inside a strong spatiotemporal modulation of the gas refractive index.

A spectral analysis of the probe (not shown) has been also performed. The resulting spectrum shows a complex evolution with respect to the case of maximum molecular alignment. In particular, the temporal slice propagating along the axis is spectrally broadened, but also shifted to the red; this effect can be explained taking into account that the slice is shorter than the initial pulse, but the temporal phase along the slice changes in a monotonic way (as can be inferred from panel B of Fig. 17) thus producing a spectral shift. On the other hand the larger part of the probe, deflected from the axis, experiences a much smaller spectral broadening with respect to that observed for maximum alignment, since it leaves the area of maximum FFA earlier.

Numerical simulations were also performed for the configuration with pump and probe having perpendicular polarizations (not shown). As expected from experiments, the spatiotemporal probe modulation is weaker with respect to the parallel polarizations case. In particular, for a pump-probe delay of 4.27 ps (thus, at molecular antialignment), we reproduced the spatial probe confinement along the wake axis. The spectral broadening resulting from simulations is about half that found in parallel configuration ($\beta=5.1$), thus in good agreement with the measured value.

E. Birefringence effects

According to experimental and theoretical results previously exposed, FA-FFA induces a transient, delayed birefringence in a gas of linear molecules; after excitation, the optical properties of the gas change both in temporal and spatial domains. As far as the polarization direction of the delayed probe is parallel or perpendicular to the molecular alignment axis, such changes do not affect the probe polarization state. In those cases, spectral broadening and spatial reshaping are the only visible effects on the probe.

A very different situation can be predicted in the case of a probe pulse with arbitrary direction of the initial polarization. Two scenarios can be envisaged, according to the degree of rotational excitation of the medium.

(i) For a mild molecular alignment, the spatial modulation induced on the probe would be weak and the excited medium could be simply modeled as a transient birefringent plate. The most significant effect would be probe spectral broadening and temporal modulation of probe polarization state in correspondence of rotational revivals. A similar effect has been also reported in argon [35]; it must be pointed out that birefringence effects in atomic gases can be induced only by cross-phase modulation due to the instantaneous Kerr effect.

(ii) Stronger rotational excitation could induce a noticeable spatial modulation of the probe: in this case, according to the previous discussion, one could observe the occurrence of polarizations separation in coincidence of rotational revivals. In particular, at maximum alignment, the probe component parallel to the alignment direction would collapse on the filament axis, whereas defocusing of the perpendicular component would occur. The opposite behavior should be observed at antialignment. As a matter of fact, a similar phenomenon has been already demonstrated in the copropagation of a probe pulse with a filamenting pump pulse in air [36], though in that case it was related to the cross-phase modulation induced by the instantaneous Kerr effect. It is worth noting that, since the nonlinear Kerr coefficient n_2 is positive, in the case of pump-probe temporal overlap the probe component parallel to the pump polarization always collapses on the filament axis whereas the perpendicular component is always defocused.

IV. CONCLUSIONS

Optical filamentation in molecular gases is an intriguing nonlinear effect, which induces a delayed reshaping of the gas refractive index both in temporal and spatial domains. These transient modifications in the optical properties of the gas are related to the field-free molecular alignment induced by the pump and can be effectively probed by a second optical pulse propagating inside the wake of the first one. Since temporal and spatial effects are simultaneous and cannot be disentangled, they affect in a new and unexpected way the evolution of the probe pulse.

We have shown, supported by measurements in several gases, that huge spectral broadening as well as spatial collapse and defocusing of the probe can be induced by filamentation-assisted FFA. The noticeable strength of the observed effects proves that this technique is a valid alternative for the characterization of FFA in molecular gases with respect to standard pump-probe configurations based on gas-filled hollow fibers.

On the other hand, the theoretical results here reported demonstrate that FA-FFA can be effectively exploited in

numerous kinds of spatiotemporal reshaping of laser pulses. Besides the already mentioned and experimentally observed effects, numerical simulations predict behaviors such as spatiotemporal compression and spatiotemporal slicing of laser pulses. We envisage that the birefringence induced in a molecular gas by filamentation-assisted FFA could be an additional degree of freedom to be exploited in a larger class of pulse shaping applications, like in polarization shaping or in the separation of polarization components.

ACKNOWLEDGMENT

We acknowledge the financial support from the Italian MIUR PRIN Project No. 2006027381.

[1] A. M. Zheltikov, Opt. Lett. **32**, 2052 (2007).
[2] H. Stapelfeldt and T. Seideman, Rev. Mod. Phys. **75**, 543 (2003).
[3] K. Hartinger, S. Nirmalgandhi, J. Wilson, and R. A. Bartels, Opt. Express **13**, 6919 (2005).
[4] R. A. Bartels, T. C. Weinacht, N. Wagner, M. Baertschy, C. H. Greene, M. M. Murnane, and H. C. Kapteyn, Phys. Rev. Lett. **88**, 013903 (2001).
[5] P. W. Dooley, I. V. Litvinyuk, K. F. Lee, D. M. Rayner, M. Spanner, D. M. Villeneuve, and P. B. Corkum, Phys. Rev. A **68**, 023406 (2003).
[6] R. Righini, Science **262**, 1386 (1993).
[7] V. Renard, O. Faucher, and B. Lavorel, Opt. Lett. **30**, 70 (2005).
[8] Y. H. Chen, S. Varma, A. York, and H. M. Milchberg, Opt. Express **15**, 11341 (2007).
[9] K. Hartinger and R. A. Bartels, Appl. Phys. Lett. **92**, 021126 (2008).
[10] V. Loriot, R. Tehini, E. Hertz, B. Lavorel, and O. Faucher, Phys. Rev. A **78**, 013412 (2008).
[11] V. Loriot, E. Hertz, A. Rouzée, B. Sinardet, B. Lavorel, and O. Faucher, Opt. Lett. **31**, 2897 (2006).
[12] R. Velotta, N. Hay, M. B. Mason, M. Castillejo, and J. P. Marangos, Phys. Rev. Lett. **87**, 183901 (2001).
[13] T. Kanai, S. Minemoto, and H. Sakai, Nature (London) **435**, 470 (2005).
[14] C. Vozzi, F. Calegari, E. Benedetti, J. P. Caumes, G. Sansone, S. Stagira, M. Nisoli, R. Torres, E. Heesel, N. Kajumba, J. P. Marangos, C. Altucci, and R. Velotta, Phys. Rev. Lett. **95**, 153902 (2005).
[15] J. Itatani, J. Levesque, D. Zeidler, H. Niikura, H. Pépin, J. C. Kieffer, P. B. Corkum, and D. M. Villeneuve, Nature (London) **432**, 867 (2004).
[16] K. Hartinger and R. A. Bartels, Opt. Lett. **33**, 1162 (2008).
[17] N. Zhavoronkov and G. Korn, Phys. Rev. Lett. **88**, 203901 (2002).
[18] S. I. Zaitsu, Y. Kida, and T. Imasaka, Phys. Rev. A **70**, 031801(R) (2004).
[19] I. V. Fedotov, A. D. Savvin, A. B. Fedotov, and A. M. Zheltikov, Opt. Lett. **32**, 1275 (2007).
[20] M. Comstock, V. V. Lozovoy, and M. Dantus, Chem. Phys. Lett. **372**, 739 (2003).
[21] A. G. York and H. M. Milchberg, Opt. Express **16**, 10557 (2008).
[22] J. R. Peñano, P. Sprangle, P. Serafim, B. Hafizi, and A. Ting, Phys. Rev. E **68**, 056502 (2003).
[23] E. T. J. Nibbering, G. Grillon, M. A. Franco, B. S. Prade, and A. Mysyrowicz, J. Opt. Soc. Am. B **14**, 650 (1997).
[24] S. Varma, Y.-H. Chen, and H. M. Milchberg, Phys. Rev. Lett. **101**, 205001 (2008).
[25] F. Calegari, C. Vozzi, S. Gasilov, E. Benedetti, G. Sansone, M. Nisoli, S. De Silvestri, and S. Stagira, Phys. Rev. Lett. **100**, 123006 (2008).
[26] Calculation performed with the density-functional method B3LYP in the aug-cc-pVTZ basis set; data achieved from the Computational Chemistry Comparison and Benchmark DataBase, NIST, http://cccbdb.nist.gov/
[27] A. Braun, G. Korn, X. Liu, D. Du, J. Squier, and G. Mourou, Opt. Lett. **20**, 73 (1995).
[28] J. Zhang, Z. H. Lu, and L. J. Wang, Appl. Opt. **47**, 3143 (2008).
[29] H. J. Lehmeier, W. Leupacher, and A. Penzkofer, Opt. Commun. **56**, 67 (1985).
[30] S. Champeaux and L. Bergé, Opt. Lett. **31**, 1301 (2006).
[31] The pump peak electric field at focus in vacuum is related to the assigned parameters by the relation $|\mathcal{E}_{p,f}|^2=8\sqrt{\frac{\ln(2)}{\pi^3}}\frac{\mathfrak{E}_p}{c\varepsilon_0 w_{0p}^2\tau_p}$. According to this convention, the parameters chosen for nitrogen are the following: $n_2=8.7\times10^{-24}$ m^2 bar/W; $\sigma_K=6.2\times10^{-219}$ m^{2K}/(s V^{2K}) and $K=11$ at 800 nm. Note that n_2 and σ_K depend on the convention adopted for the electric field envelope.
[32] J. Ortigoso, M. Rodriguez, M. Gupta, and B. Friedrich, J. Chem. Phys. **110**, 3870 (1999).
[33] E. Hertz, D. Daems, S. Guérin, H. R. Jauslin, B. Lavorel, and O. Faucher, Phys. Rev. A **76**, 043423 (2007).
[34] M. Leibscher, I. Sh. Averbukh, and H. Rabitz, Phys. Rev. Lett. **90**, 213001 (2003).
[35] P. Béjot, Y. Petit, L. Bonacina, J. Kasparian, M. Moret, and J.-P. Wolf, Opt. Express **16**, 7564 (2008).
[36] Y. Chen, C. Marceau, F. Théberge, M. Chteauneuf, J. Dubois, and S. L. Chin, Opt. Lett. **33**, 2731 (2008).